Computational study of $GaAs_{1-x}N_x$ and $GaN_{1-y}As_y$ alloys and arsenic impurities in GaN

2006 J. Phys.: Condens. Matter 18 10097

(http://iopscience.iop.org/0953-8984/18/44/009)

INSTITUTE OF PHYSICS PUBLISHING JOURNAL OF PHYSICS: CONDENSED MATTER

J. Phys.: Condens. Matter **18** (2006) 10097–10114 doi:10.1088/0953-8984/18/44/009

Computational study of $GaAs_{1-x}N_x$ and $GaN_{1-y}As_y$ alloys and arsenic impurities in GaN

K Laaksonen[1], H-P Komsa[2], E Arola[2], T T Rantala[2] and R M Nieminen[1]

[1] Laboratory of Physics, Helsinki University of Technology, PO Box 1100, FI-02015 HUT, Finland
[2] Institute of Physics, Tampere University of Technology, PO Box 692, FI-33101 Tampere, Finland

E-mail: katri.laaksonen@tkk.fi

Received 9 May 2006, in final form 29 September 2006
Published 20 October 2006
Online at stacks.iop.org/JPhysCM/18/10097

Abstract

We have studied the structural and electronic properties of As-rich $GaAs_{1-x}N_x$ and N-rich $GaN_{1-y}As_y$ alloys in a large composition range using first-principles methods. We have systematically investigated the effect of the impurity atom configuration near both GaAs and GaN sides of the concentration range on the total energies, lattice constants and bandgaps. The N (As) atoms, replacing substitutionally As (N) atoms in GaAs (GaN), cause the surrounding Ga atoms to relax inwards (outwards), making the Ga–N (Ga–As) bond length about 15% shorter (longer) than the corresponding Ga–As (Ga–N) bond length in GaAs (GaN). The total energies of the relaxed alloy supercells and the bandgaps experience large fluctuations within different configurations and these fluctuations grow stronger if the impurity concentration is increased. Substituting As atoms with N in GaAs induces modifications near the conduction band minimum, while substituting N atoms with As in GaN modifies the states near the valence band maximum. Both lead to bandgap reduction, which is at first rapid but later slows down. The relative size of the fluctuations is much larger in the case of $GaAs_{1-x}N_x$ alloys. We have also looked into the question of which substitutional site (Ga or N) As occupies in GaN. We find that under Ga-rich conditions arsenic prefers the substitutional N site over the Ga site within a large range of Fermi level values.

1. Introduction

The III–V compound semiconductors have been the focus of a major research effort in the recent years. In the case of As-rich $GaAs_{1-x}N_x$ and N-rich $GaN_{1-y}As_y$ alloys, one important reason for this interest is their capability to produce light in a wavelength region which reaches from infrared to ultraviolet. This makes them very attractive e.g. for optoelectronic applications.

Many compound semiconductor alloys show band bowing, i.e. their bandgaps change in a nonlinear way between the bandgaps of the binary alloys. For the GaAsN alloys this effect is very strong, which allows large changes in the bandgap value with a small change in composition [1]. The reason for this, as well as for other properties which differ from more conventional III–V semiconductors, has been attributed to the large size mismatch between the fifth column components, arsenic and nitrogen [2]. As-rich $GaAs_{1-x}N_x$ alloys have already been studied extensively both experimentally and theoretically, but N-rich alloys have only relatively recently started to attract more attention.

Most of the recent studies have concentrated only on either As-rich or N-rich alloys, since only low nitrogen concentrations in GaAs or arsenic concentrations in GaN can be reached experimentally. The reason for this is the existence of a large miscibility gap in this alloy [3, 4], caused by the large lattice constant mismatch between GaAs and GaN [5]. However, the behaviour of the bandgap has been theoretically studied over the whole concentration range and the bandgap bowing parameter has been found to be strongly concentration dependent [2, 6]. Recently, Carrier *et al* studied the structural properties of both dilute-As and dilute-N regimes of GaAsN alloys [7].

In the As-rich $GaAs_{1-x}N_x$ alloys the nitrogen concentration in a bulk material is limited to a few per cent [8], although in thin films it can be substantially larger [3, 8, 9]. In bulk-like samples, where the layer thickness is more than 0.5 μm, typical nitrogen concentrations are lower than 3% [10, 11]. However, in thin film samples, where the layer thickness is less than 0.5 μm, nitrogen concentration can be close to 20% [3, 8] and in some cases GaAsN alloys with 30% nitrogen can be reached [9].

In As-rich $GaAs_{1-x}N_x$ alloys bandgap measurements have revealed a fast reduction of the bandgap energy when the N concentration is increased from zero to a few per cent and the reduction has been found to slow down for higher N concentrations. This means that the bandgap bowing parameter has a strong composition dependence for small N concentrations [4, 8], which is also supported by theoretical findings [12, 6, 5, 13, 14].

Most of the nitrogen atoms in GaAs incorporate at As sites, although in several experimental studies it has been shown that single N atoms and N–N dimers can also be found in different interstitial sites [15–17]. In many theoretical studies the nitrogen atoms have been assumed to be in the As sites [18, 13, 14, 19], but recently there have been several defect studies which have also considered different interstitial type defects [18, 7, 20].

The N-rich $GaN_{1-y}As_y$ alloys have been theoretically little studied so far. Arsenic defects in GaN were first investigated using a first-principles method by Mattila and Zunger, who calculated the defect energy and ionization levels of As substitutional defects on the N site and found that As induces deep levels in the bandgap [21]. The arsenic incorporation to the nitrogen site was implicitly assumed until Van de Walle and Neugebauer investigated the possibility of arsenic incorporation also at the Ga sites and found As to prefer the Ga site in p-type materials (Fermi level E_F below 2.3 eV) [22]. The defect formation energies and ionization levels of both As_N and As_{Ga} have also been studied by Ramos *et al* [23].

Novikov *et al* [24] and Foxon *et al* [25] studied samples with As concentration up to 0.2% grown with the molecular beam epitaxy (MBE) technique using photoluminescence (PL). Samples grown with high Ga flux showed the two known strong emission bands: band edge emission at 3.4 eV and blue emission centred at 2.6 eV. The energy of the band-edge emission was close to the GaN bandgap energy, and also the lattice parameters of these samples were close to those of GaN. If the Ga flux was low the emission intensities decreased by several orders of magnitude in the case of the blue emission, and by one order of magnitude in the case of the band-edge emission. Also the position of the band-edge emission moved to lower energy and the lattice constant changed. Based on these observations they concluded that a high N/Ga

ratio, i.e. more N-rich conditions, is needed in order to grow N-rich $GaN_{1-y}As_y$ alloys, which is in contradiction with the theoretical prediction by Van de Walle and Neugebauer [22].

Recently, several groups have reported the growth of N-rich $GaN_{1-y}As_y$ alloys with a high (over 3%) concentration of arsenic. Kimura *et al* had grown $GaN_{1-y}As_y$ with up to 6.7% As using the metallorganic vapour phase epitaxy (MOVPE) technique. They studied the samples using optical absorption spectroscopy and determined the bandgap bowing parameter for the alloy from the bandgap energies decreasing from 3.39 eV (GaN) to approximately 2.25 eV (see figure 3 of [26]) while As concentrations changed from 0 to 6.7% [27, 26]. Wu *et al* [28] grew samples with As concentration ranging from 0 to 6% by using MOVPE and studied the optical transitions using photomodulated transmission. They interpreted the emission with the energy of 2.6–2.7 eV to derive from the As_N defect, based on the computational result by Mattila and Zunger [21] that the As_N defect has an energy level at about 0.4 eV above the VBM. They used the hybridization of this level with the GaN valence band states in order to explain the composition dependence of the bandgap in the $GaN_{1-y}As_y$ alloys. Tsuda *et al* [29] grew N-rich $GaN_{1-y}As_y$ alloys with As concentration up to 4.3% using the metallorganic chemical vapour deposition (MOCVD) technique, and studied them using cathodoluminescence spectroscopy (CL). They observed both the near band-edge emission and blue emission, which both showed band bowing. Based on the computational results by Van de Walle and Neugebauer [22], they then considered the blue luminescence related localized state feature to be probably due to the As_{Ga} defect.

In the following the notations $GaAs_{1-x}N_x$ (where x is small) and $GaN_{1-y}As_y$ (where y is small) refer to alloys with As- and N-rich composition, respectively. We present the computational method in section 2, then our results for the $GaAs_{1-x}N_x$ and $GaN_{1-y}As_y$ alloys and As defects in GaN in section 3 and finally in section 4 our conclusions. Section 3 is divided into three parts. The first and second parts deal with the effects of alloying on the properties of $GaAs_{1-x}N_x$ and $GaN_{1-y}As_y$ alloys, respectively. We investigate how the configuration of the impurity atoms affects the structure, energetics and electronic properties of the alloy. We also show how the impurity states near the conduction band minimum in the As-rich alloy and near the valence band maximum in the N-rich alloy affect the bandgap in different ways in the two different composition regions as the impurity concentration increases. We compare our results for $GaAs_{1-x}N_x$ alloys to previous theoretical and experimental results (for example, our densities of states to recent ballistic emission electron microscopy (BEEM) results [30]). There are very few previous theoretical studies concentrating on the $GaN_{1-y}As_y$ alloys and we present comprehensive results concerning their structural and electronic properties. Since it is not yet clear from theoretical or experimental studies if As would indeed incorporate on the N site in GaN and how to interpret the experimental findings, we also look into this question in the last part of section 3. We find that under Ga-rich conditions arsenic would prefer the substitutional N site over the substitutional Ga site within a large range of Fermi level values.

2. Methods

The calculations have been performed using the density-functional theory based code VASP (Vienna *Ab Initio* Simulation Package) with the projector augmented wave (PAW) method [31] and the local density approximation (LDA) [32]. We also considered the possibility of using the generalized gradient approximation (GGA) [33], but found that it gives even smaller values than the LDA for the bandgap, which would have caused additional problems in the alloy calculations. For example, for GaAs the LDA gives 0.53 eV for the bandgap while the GGA gives only 0.13 eV (the experimental value is 1.43 eV [34]). This problem can probably be

Table 1. Substitutional impurity atom (X) positions in a 64-atom supercell for different configurations used in the alloy calculations for $GaY_{1-z}X_z$, where X and Y denote N or As and z is the impurity concentration. Other V-sublattice sites are occupied by the host atoms (Y). In total there are 32 sites in the V sublattice.

Composition	z (%)	1	2	3	4
X_1Y_{31}	3.125	(0, 0, 0)			
X_2Y_{30}[110]	6.250	(0, 0, 0)	(0, 1, 1)		
X_2Y_{30}[200]	6.250	(0, 0, 0)	(2, 0, 0)		
X_2Y_{30}[211]	6.250	(0, 0, 0)	(2, 1, 1)		
X_2Y_{30}[220]	6.250	(0, 0, 0)	(2, 2, 0)		
X_2Y_{30}[222]	6.250	(0, 0, 0)	(2, 2, 2)		
X_3Y_{29}[a]	9.375	(0, 0, 0)	(3, 2, 1)	(1, 3, 2)	
X_3Y_{29}[b]	9.375	(0, 0, 2)	(2, 0, 0)	(2, 2, 2)	
X_4Y_{28}[a]	12.500	(0, 0, 0)	(3, 2, 1)	(1, 3, 2)	(2, 1, 3)
X_4Y_{28}[b]	12.500	(0, 3, 1)	(2, 3, 3)	(0, 1, 3)	(2, 1, 1)

related to the large lattice constant that the GGA gives (5.75 Å, while the LDA gives 5.61 Å, and the experimental value is 5.64 Å [34]).

We have done all the alloy calculations using the zinc-blende crystal structure, while studies of GaN and its defects have been carried out using both the zinc-blende and wurtzite structures. We have used a 64-atom supercell with the **k**-point sampling of the Monkhorst–Pack $2 \times 2 \times 2$ scheme, and a 216-atom supercell with a single **k** point in the calculations done using the zinc-blende structure. The gallium $3d$ states were included as valence states. In the alloy calculations the cut-off energy was 400 eV. For each configuration, in the 64-atom supercell case, we performed structural relaxation and determined the lattice parameter computationally using the Murnaghan equation of state. For the 216-atom supercell case of the $GaAs_{1-x}N_x$ alloy ($x = 0.926\%$), the lattice constant was taken from linear interpolation between the lattice constants of GaAs and GaN, after a linear dependence on the composition was found using the smaller 64-atom supercell.

In the defect calculations for arsenic in GaN we performed the ion relaxation, but used the theoretical lattice constant corresponding to pure GaN. The investigated defect cases are As on a nitrogen site and As on a gallium site as a substitutional defect. Both defects were calculated in three different charge states: neutral, 1+ and 2+. For the charged cases, a neutralizing uniform background was introduced to the supercell. No Madelung corrections were applied. The formation energy of these defects was calculated in both zinc-blende and wurtzite structures. In the cases of the zinc-blende and wurtzite crystal structures we used 64-atom cubic and 96-atom orthorhombic supercells, respectively. In both cases the **k**-point sampling was based on the $2 \times 2 \times 2$ scheme. The cut-off energy in these calculations was 500 eV.

In order to probe atomic short-range order effects on electronic and structural properties of $GaAs_{1-x}N_x$ and $GaN_{1-y}As_y$ alloys we have used the atomic configurations given in table 1 and figure 1. All impurity atoms have been placed substitutionally in the group-V sublattice of GaN and GaAs in the cases of N- and As-rich alloys, respectively. In the following sections we have used the notation introduced in table 1 for $GaY_{1-z}X_z$, where Y and X stand for N (As) and As (N), respectively, for the N- (As-) rich alloy, and z is the impurity concentration.

For one and two impurity atoms in a 64-atom supercell we have studied all possible configurations (one for X_1Y_{31} and five for X_2Y_{30}). In order to study alloys with higher concentrations of impurity atoms we have chosen two different configurations marked with [a] and [b] for both X_3Y_{29} and X_4Y_{28} compositions. All these configurations are of the same type in the sense that the atoms have been placed relatively far apart from each other and there are no clusters.

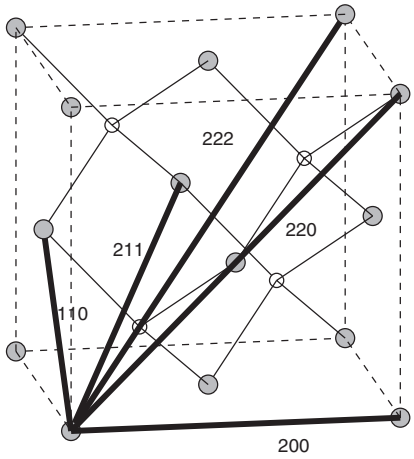

Figure 1. Positions of the two impurity atoms used in the calculations of various As_2N_{30} and N_2As_{30} configuration cases. One-eighth of the 64-atom supercell used in the calculations is shown.

Table 2. The lattice constant a, the total energy E_{rel} of the supercell, the bulk modulus B and the bandgap E_g of GaAs and the relaxed structures of the $GaAs_{1-x}N_x$ alloys with various N atomic configurations. Also shown is the total energy E_{nonrel} related to the nonrelaxed (GaAs) crystal structure. For the notation of the configurations see table 1 and figure 1.

Composition	N%	a (Å)	E_{nonrel} (eV)	E_{rel} (eV)	B (GPa)	E_g (eV)
GaAs	0	5.61	−306.81		74	0.53
N_1As_{107}	0.926	5.597	−1034.76	−1038.87		0.40
N_1As_{31}	3.125	5.57	−307.52	−309.65	78	0.14
N_2As_{30}[110]	6.250	5.535	−308.23	−312.36	78	
N_2As_{30}[200]	6.250	5.535	−308.23	−312.64	77	0.24
N_2As_{30}[211]	6.250	5.535	−308.23	−312.65	77	0.02
N_2As_{30}[220]	6.250	5.535	−308.22	−312.17	78	
N_2As_{30}[222]	6.250	5.535	−308.23	−312.72	74	0.12
N_3As_{29}[a]	9.375	5.50	−309.55	−315.89	81	
N_3As_{29}[b]	9.375	5.50	−309.52	−314.32	79	

3. Results and discussion

3.1. As-rich $GaAs_{1-x}N_x$ alloys

First we discuss the total energy, structural properties, bulk modulus and electronic structure of As-rich $GaAs_{1-x}N_x$ substitutional alloys for various N compositions and atomic configurations. Table 2 presents the computational results for the lattice constant a, the total energy E_{rel} of the supercell, the bulk modulus B and the bandgap E_g of GaAs and the relaxed structures of As-rich $GaAs_{1-x}N_x$ alloys with various N atomic configurations. Also shown is the total energy related to the nonrelaxed crystal structure (E_{nonrel}).

We observe from the calculations that the lattice constant behaves linearly when moving from GaAs to GaN. The bulk modulus also increases steadily, although with an increasing amount of fluctuation, while adding nitrogen. In the case of two N atoms in the supercell, corresponding to the 6.25% N concentration, the N_2As_{30}[222] configuration is energetically the lowest one, and the configurations in the [110] and [220] directions are the most unfavoured ones. These total energy considerations suggest that the substitutional nitrogen atoms prefer to form alloys with large distances between the N atoms. These observations agree with the results from the empirical pseudopotential (EPM) and valence force field (VFF) models for clusters by

Kent and Zunger [19]. With three substitutional nitrogens the [a] configuration is clearly more favourable than the [b] one. This is understandable since the [a] configuration contains mostly [211] nitrogen pairs, which lead to a low-energy state in the N_2As_{30} calculations, while the [b] configuration contains mostly [220] nitrogen pairs, which have almost 0.5 eV higher energy in the N_2As_{30} calculations. Interestingly, all the total energies between the different nonrelaxed configurations are very close to each other. Therefore, the total energies for different relaxed N atomic configurations in table 2 should directly indicate the amount of host atomic relaxation associated with the relaxation.

Due to the nitrogen being much smaller than arsenic, there is a large geometric relaxation around the nitrogen atom. In the N_1As_{31} case the Ga–N bond length is 15% shorter than the Ga–As bond length for a GaAs supercell of the same lattice constant. The size of the relaxation also stays practically the same with all the N_2As_{30} and N_3As_{29} configurations. Our calculations show that relaxation is governed by the nitrogen positions in such a way that when the nitrogen atoms are furthest apart from each other, the lattice has the largest freedom to relax. On the other hand, in the N_2As_{30}[220] case, the arsenic atoms located in the same plane as the nitrogen atoms do not move, since they are pulled by both nitrogens symmetrically over the supercell boundaries.

In the N_1As_{31} case, as well as in all the N_2As_{30} cases, apart from the [110] case, the nitrogens stay in the same positions as the arsenics they substitute, and only the lattice around them becomes relaxed. In the N_2As_{30}[110] case, the nitrogen atoms prefer to get closer to each other, and to form a strongly bonded dimer, but the lattice prevents this. However, the distance between the nitrogen atoms decreases by about 6%. The N_2As_{30}[200] configuration generates nitrogen chains which prohibit movement of the nitrogen atoms, but which allow other atoms to relax rather freely. McKay *et al* [35] have studied the distribution of N–N pairs near the $GaAs_{0.983}N_{0.017}$ alloy surface, as a function of the N–N separation and direction by using scanning tunnelling microscopy. They have observed that the [001]-oriented second-nearest-neighbour pairs, which correspond to our N–N pairs with the [200] configuration, occur more frequently than the other types of N–N pairs.

Ciatto *et al* [36] studied the average bond lengths in As-rich GaAsN alloys both experimentally using the XAFS method and theoretically using a computational method that is very similar to the one we used (VASP code with the PAW method and LDA). They note that the average Ga–As and Ga–N bond lengths decrease with increasing N content for an unstrained alloy but increase for a strained alloy. We have only studied the unstrained alloys and find a similar decrease in the bond lengths with increasing N concentration for most of the configurations (the exceptions were the ones with chains of atoms in the [110]-direction, which were found to be energetically unfavourable. They were also not included in the theoretical studies in the paper by Ciatto *et al*.) The thin GaAsN alloy layers with a high impurity concentration are usually strained, which means that their average bond lengths will behave differently as a function of the N content from our unstrained alloys. For this reason we do not present our results for the average bond lengths in detail in this paper.

3.1.1. Band structure. In the following we discuss the modifications occurring in the electronic structure of the GaAs crystal with the zinc-blende structure, when As atoms in the V sublattice are substitutionally being replaced by isovalent N atoms.

The values of the energy gap and the bowing parameter depend on the configuration of N atoms in the supercell for a given concentration, reflecting the details of the bonding properties. It can be seen from table 2 that adding N to the group-V sublattice of GaAs between 0.926% and 9.375% drastically reduces the calculated bandgap from its value for GaAs. Although it is well known that the DFT theory within the framework of the local density approximation

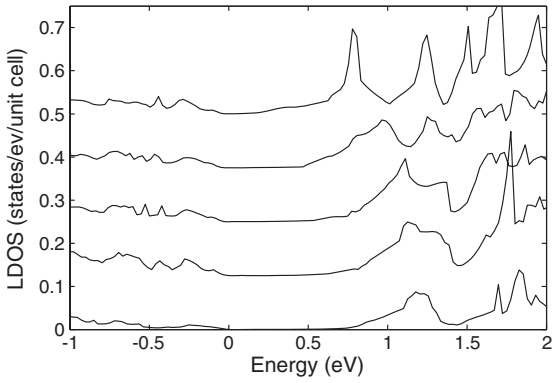

Figure 2. Evolution of the nitrogen local DOS for various N atomic configurations of the N_2As_{30} case. From the bottom to the top: N_2As_{30}[222], N_2As_{30}[200], N_2As_{30}[211], N_2As_{30}[110], and N_2As_{30}[220]. For the notation of the configurations see table 1 and figure 1.

(LDA) greatly underestimates the bandgap (e.g., the experimental value is 1.43 eV [34] for GaAs, while our calculated value is only 0.53 eV), the DFT calculations within the LDA or GGA approximations are supposed to predict the trends in the single-particle energies quite accurately. However, the bandgap becomes negative at 9.375% nitrogen concentration, as well as with some N atomic configurations even at 6.25%. Our calculations also show that if a hydrostatic external pressure is applied the bandgap will open, and since the bandgap opening as a function of pressure seems to stay rather constant (0.045 eV GPa^{-1}) at low pressures we can estimate the pressures needed to open the bandgap in these cases. The pressures are 7.8 and 4.4 GPa for the N_2As_{30}[110] and N_2As_{30}[220] configurations, respectively.

Estimation of the bandgap for a $GaAs_{1-x}N_x$ random alloy with an $x = 6.25\%$ concentration is a difficult task. Simple averaging is incorrect, since our ordered phase calculations cannot be used to predict the random phase bandgap. However, the three lowest energy N atomic configurations ([200], [211] and [222]) most likely define the range for the estimate, but have bandgaps ranging over 200 meV. We choose the lowest energy configuration ([222]) related bandgap (0.12 eV), which is also quite close to the average value of the bandgaps for the three lowest energy configurations.

It is interesting to notice that the bandgap in the case of the N_2As_{30}[200] configuration becomes larger than in the N_1As_{31} case. A tentative reason for this is the fact that the conduction band edge (CBE) in the N_2As_{30}[200] case experiences a notably weaker nitrogen localization than in the N_1As_{31} case, as can be deduced from figure 2.

Experimental bandgap values as measured, for example, by Uesugi *et al* [37] lead to bandgap decrements of approximately 0.15, 0.35, and 0.55 eV, for the 0.926%, 3.125%, and 6.25% nitrogen concentrations, respectively. Our calculated corresponding values are 0.13, 0.39, and 0.43 eV, showing the same trend as experiments. With the bandgap estimate of 0.12 eV for the 6.25% concentration case, it is obvious that the closeness of the valence band pushes the conduction band upwards excessively. It is clear from table 2 that the bandgap values experience large fluctuations with different atomic configurations of N. Large bandgap fluctuations were also measured and computationally verified recently in a similar fashion by Bentoumi *et al* [38]. Although the bandgap fluctuations are large, the lowest-energy configurations clearly indicate that the bandgap decreases rapidly for small N concentrations and then slows down for larger ones.

For N_1As_{31}, N_2As_{30}[222], and N_2As_{30}[110] configurations the band structures are shown in figure 3. Nitrogen localized states form the lowest conduction band, which is clearly separated from the other conduction bands. This band is similar to the lowest GaAs conduction band, but as the nitrogen concentration increases it is pushed down in energy. With several

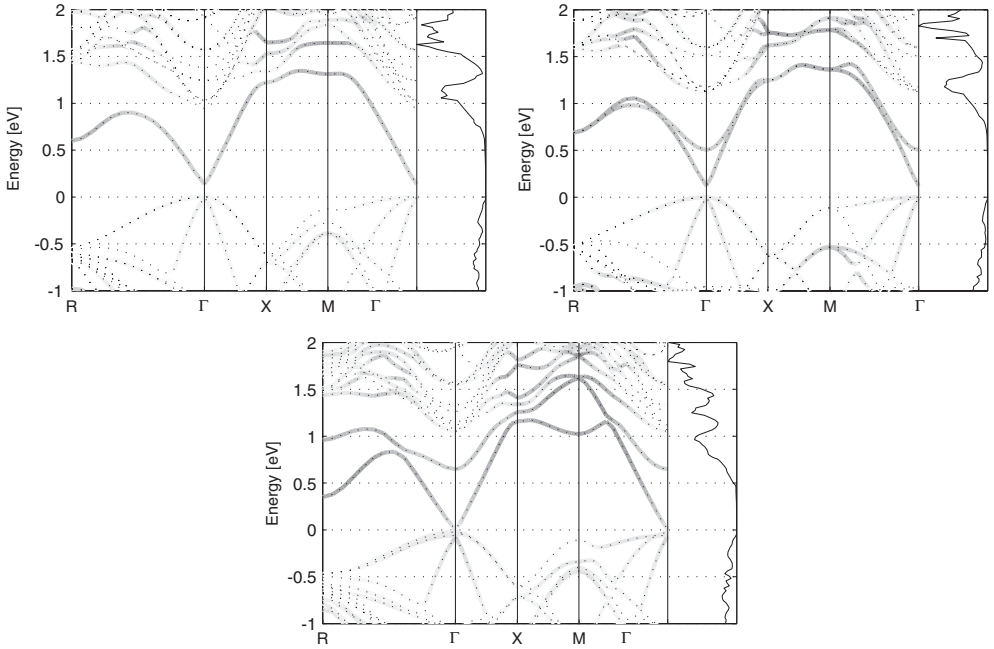

Figure 3. The band structures of the N_1As_{31} (top left), N_2As_{30}[222] (top right), and N_2As_{30}[110] (bottom) cases. The extent of the N localization is depicted by shading the band lines. On the right is the respective nitrogen local DOS. For the notation of the configurations see table 1 and figure 1.

nitrogen atoms in the computational cell the impurity band degenerates and splits according to the nitrogen separation and interaction (orientation, see figure 1).

Interestingly, in the cases with a single nitrogen atom and a nitrogen dimer related interstitial defect, the bandgap varies only slightly for different local environments of the defect. The nitrogen dimer interstitials at the centre of the Ga- or As-related tetrahedron lead to a tiny redshift effect, the bandgap reduction being of the order of 30 meV. On the other hand, the Ga tetrahedron edge-related single N impurity interstitial causes a substantial blueshift effect, increasing the bandgap by some 200 meV as compared to that of the GaAs crystal [20].

3.1.2. Density of states. Comparison of the densities of states (DOS) in the N_1As_{107}, N_1As_{31}, and N_2As_{30}[222] cases reveals very similar characteristics. In figure 4 we have plotted nitrogen local DOS curves, as a function of increasing nitrogen concentration, in order to better visualize the interesting features. It clearly shows how the lowest conduction band states are nitrogen localized and form a strongly nitrogen localized peak at about 1 eV above the valence band maximum (VBM), between $x = 0.926\%$ and 6.25%. The evolution of this peak through different concentrations is quite independent of the supercell size, which therefore enables us reliably to interpret this feature. We also observe from figure 4 that the valence band nitrogen localization is small, which partially explains why it does not change drastically when the composition is changed.

Additionally, the N_2As_{106}[110] calculations (not explicitly included in this paper) show a very similar nitrogen local DOS peak to the N_2As_{30}[110] case, proving the intercell effects to be small in the case of this peak.

Nitrogen localization increases when going from the N_2As_{30}[222] configuration to the N_2As_{30}[220] one, and decreases when going to all the other configurations. The greater

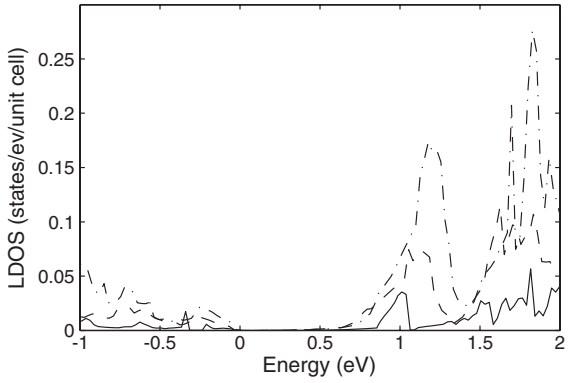

Figure 4. Nitrogen local DOS evolution in $GaAs_{1-x}N_x$ solid solutions. Solid, dashed, and dash–dotted lines correspond to N_1As_{107} ($x = 0.926\%$), N_1As_{31} ($x = 3.125\%$), and N_2As_{30}[222] ($x = 6.25\%$) N atomic configurations (concentrations), respectively. For the notation of the configurations see table 1 and figure 1.

N_2As_{30}[220] localization over the N_2As_{30}[110] one is probably due to the small geometry relaxation; i.e., the neighbouring gallium atoms are further away from the nitrogen atom, leading to a smaller hybridization. This can be seen by looking at the localized nitrogen wavefunctions, which have tails in the [110] directions. These results are in agreement with the calculations by Al-Yacoub and Bellaiche [39], who studied nitrogen chains in the $In_{0.05}Ga_{0.95}As_{0.984}N_{0.016}$ alloy, using the empirical pseudopotential method (EPM) combined with the valence force field (VFF) method. Also, the bandgap behaviour with respect to the N_2As_{30}[200] and N_2As_{30}[220] configurations is qualitatively similar to that found by Al-Yacoub and Bellaiche (see table III of [39]).

In the case of the N_1As_{31} N atomic configuration the character of the nitrogen localized peak can be deduced from the density-of-states curves of figures 3 and 4. We observe from figure 3 that the DOS curve above the conduction band edge (CBE) first rises slowly, then after the *R*-valley it starts to rise more rapidly, and finally has an additional increase (or a hump) in the energy region, where folded GaAs derived states at the Γ-point are being included. However, the nitrogen localization of these states is very low, and we also observe that the **k**-space integration, near the Γ point, has only a minor contribution to the DOS peak. However, our calculations show that the hump in the DOS curve, around 1 eV above the CBE, is due to fairly localized features (not shown in this paper) in the electronic band structure along a general **k** direction in the Brillouin zone.

Our calculations also show, regarding the nature of the N localized DOS peak near 1 eV above the VBM, that the situation with the N_1As_{107} and N_2As_{30}[222] atomic configurations is very similar to the N_1As_{31} one (see figure 4). However, in the case of the N_2As_{30}[110] atomic configuration, the nitrogen derived conduction bands, around 1 eV above the VBM, experience a strong repulsion, which consequently creates the two peaks seen in the DOS curve of the N_1As_{31} configuration (see figure 3).

A further comparison of different N atomic configurations with the 6.25% nitrogen concentration is presented in figure 2. The configurations are seen to lose the single-peak structure in their DOS curves around 1 eV, which then becomes split into two peaks when the nitrogen atoms are brought close to each other.

There are obviously only a few experimental DOS measurements carried out for GaAsN alloys. Kozhevnikov *et al* [30] used the ballistic electron emission microscopy (BEEM) technique [40], and found three peaks in the second-derivative BEEM (SD-BEEM) spectra of the transmission current. These features should correspond to the edges of particular band-structure valleys. A more thorough explanation of the BEEM technique, and how it is related to the DOS, is included as an appendix. The experiments showed two distinct main peaks

throughout the whole examined nitrogen composition range of 0–2%, and additionally a weaker one, which becomes visible at about 1% (see figure 2 of [30]). The first peak was shifted rapidly toward lower energies (voltages) when the nitrogen concentration increased, and was straightforward to assign to the conduction band minimum (Γ-like). The second peak stayed at about a constant energy, only slowly moving toward higher energies while the nitrogen concentration was increased. Its strongest contribution was assigned to the L-like $t_2(L_{1c})$ triplet state. The intensity of this peak decreased substantially as the nitrogen concentration was increased, which demonstrates that the peak cannot be identified as a localized N related resonant state (otherwise its intensity should increase due to larger values of the DOS). The faint third peak, which was observed at $x = 1.2\%$ and 1.7%, located ∼0.40 and ∼0.43 eV above the Γ-like peak, respectively, and was tentatively associated with the $a_1(L_{1c})$ singlet state.

Our calculations, at 0.926% nitrogen concentration, show a rather sharp DOS peak (not shown in this paper), starting from about 0.5 eV above the CBM (1 eV above the VBM). It is located near the GaAs-derived L_1-symmetric lowest conduction band states. As discussed above, by direct comparison to the nitrogen local DOS (see figure 4), one could also argue that this peak is related to the N-derived localized states of the lowest conduction band. However, this is unlikely, since the DOS peak in question would then gain intensity with increasing nitrogen concentration, and this would contradict the recent experiments (see, for example, figure 2 of [30]).

A faint DOS peak, which we expect to be related to the faint SD-BEEM feature in figure 2 of [30] about 0.4 eV above the CBM, cannot be observed from our DOS calculation, at 0.926% nitrogen concentration. However, our computed electronic band structure (not shown in this paper) at the same N concentration reveals a nitrogen derived band related L valley, at about 0.35 eV above the CBM.

On the basis of our DOS and electronic band structure calculations for the $x = 0.926\%$ nitrogen concentration case, as discussed above, we agree with the interpretation of Kozhevnikov *et al* [30] about the nature of the two major peaks and one weak one seen in the experimental SD-BEEM spectra of [30], for nitrogen compositions $x = 1.2\%$ and 1.7%. Namely, the largest contribution to the lowest- and highest-energy major BEEM peaks derives from the Γ- and $t_2(L_{1c})$-like triplet states, respectively, while the weak peak, between these two, can be associated mainly with the $a_1(L_{1c})$-like singlet state. However, one needs to be careful when assigning various BEEM spectral features with labels such as $t_2(L_{1c})$ and $a_1(L_{1c})$, because strictly speaking these symbols are related to symmetry groups of an isolated nitrogen in an otherwise perfect host GaAs crystal, i.e. to the ultradilute limit of the $GaAs_{1-x}N_x$ alloy.

Finally, we notice, when looking at the nitrogen localization on the basis of the nitrogen local density of states in $GaAs_{1-x}N_x$ alloys for $x = 0.926\%$, 3.125%, and 6.250% compositions, that the L-like states (relevant for the L-like SD-BEEM peak of [30]) lose nitrogen localization as the composition increases, while the $a_1(L_{1c})$-like states (relevant for the faint SD-BEEM peak of [30]) gain nitrogen localization.

3.2. N-rich $GaN_{1-y}As_y$ alloys

The total energy, structural properties, bulk modulus, and electronic structure of N-rich $GaN_{1-y}As_y$ substitutional alloys for various As compositions and atomic configurations will be discussed in the following.

Table 3 presents the computational results for the lattice constant a, total energy E_{rel} of the supercell, and the bulk modulus B of GaN and the relaxed structures of N-rich $GaN_{1-y}As_y$ alloys with various As atomic configurations. Also shown is the total energy related to the nonrelaxed (GaN) crystal structure (E_{nonrel}).

Table 3. The lattice constant a, the total energy E_{rel} of the supercell, the bulk modulus B and bandgap (E_{g}) of GaN and relaxed structures of $GaN_{1-y}As_y$ alloys with various As atomic configurations. Also shown is the total energy E_{nonrel} related to the nonrelaxed (GaN) crystal structure. For the notation of the configurations see table 1 and figure 1.

Composition	As%	a (Å)	E_{nonrel} (eV)	E_{rel} (eV)	B (GPa)	E_{g} (eV)
GaN	0	4.461	−445.97		198	1.93
As_1N_{31}	3.125	4.494	−433.91	−438.89	194	1.44
As_2N_{30}[110]	6.250	4.529	−422.62	−432.17	185	0.70
As_2N_{30}[200]	6.250	4.529	−422.73	−432.29	186	1.20
As_2N_{30}[211]	6.250	4.529	−422.73	−432.22	186	1.27
As_2N_{30}[220]	6.250	4.531	−422.78	−431.41	183	0.70
As_2N_{30}[222]	6.250	4.528	−422.72	−432.22	185	1.16
As_3N_{29}[a]	9.375	4.563	−412.47	−425.91	179	1.18
As_3N_{29}[b]	9.375	4.572	−412.54	−423.52	176	0.30
As_4N_{28}[a]	12.500	4.598	−403.05	−419.89	170	1.18
As_4N_{28}[b]	12.500	4.615	−403.24	−415.36	164	

It can be seen from table 3 that the lattice constant increases rather linearly with As concentration. For example, our calculated lattice constant for the 3% As case is 0.07% smaller than the value we get from a linear interpolation between the lattice constants of GaN and GaAs. Carrier *et al* [7] found a difference of similar size but their calculated lattice constant is larger instead of smaller than the interpolated one. Interestingly, unlike the nonrelaxed energies (E_{nonrel}), which possess very similar values for different As atomic configurations, the total energies (E_{rel}) of the relaxed lattice experience substantial variation among the different configurations for a given concentration.

There is a large size difference between an arsenic atom and a nitrogen atom. Consequently, if a N atom is replaced with an As atom the surrounding Ga atoms move outwards, away from the As atom. We have calculated the relaxations of the atoms in the alloy supercell by comparing the distance between two neighbouring atoms in the alloy supercell to a distance between the two neighbouring atoms in the equivalent positions of the zinc-blende crystal which has the same lattice constant. For As_1N_{31} the relaxations of the nearest neighbour Ga atoms are 15.2%. In alloys with a higher concentration of arsenic the relaxations are slightly smaller.

In the As_2N_{30}[222] configuration the pair formed by the arsenic atoms is in the (111) direction and the Ga atoms between these As atoms relax less (14.8%) than the other nearest neighbour Ga atoms (15.1%). In the As_2N_{30}[110] case the two As atoms form a next-nearest-neighbour pair, and there is a Ga atom which is a nearest neighbour to both of them. This Ga atom moves away from the As atoms in the direction which is perpendicular to the As pair. In the configuration As_2N_{30}[220] which has the highest energy, the As atoms are placed in the corner and in the middle of one of the faces of the supercell. It turns out that the relaxation of the atomic positions cannot happen freely in the (100) planes in this case. This leads to an isotropic change in the lattice parameters of the supercell, the lattice constant becoming a bit larger than in the other configuration cases (see table 3). Since the cell shape is not allowed to change, this creates a rather rigid three-dimensional structure and the nearest-neighbour Ga atoms can only relax by 13.2%. Similar behaviour was found in the N_2As_{30}[220] case (see section 3.1). In the As_2N_{30}[200] case the two As atoms are placed on one edge of the supercell. They are relatively far apart from each other, and there are no Ga or N atoms directly between them. This allows a substantial lowering of energy by the local structural relaxation. For each of the As atoms one of the nearest neighbour Ga atoms moves slightly less (14.8%) than the others (15.0%). In the As_2N_{30}[211] case, too, the As atoms are far apart from each other and

no other atoms are directly between them, therefore leading to a large drop of the total energy during relaxation.

In the As_3N_{29} and As_4N_{28} configurations marked with [a] there are mostly [211]-type pairs, while in those marked with [b] there are [220]-type pairs. If we look at the energies, the As_2N_{30}[211] configuration has a rather low energy, and the As_2N_{30}[220] one has the highest energy of the all of the configurations with the same arsenic concentration. It turns out that the [a] and [b] configurations of the As_3N_{29} and As_4N_{28} cases also have lower and higher energies, respectively. From table 3 the same kind of similarity can be seen in the behaviour of the lattice constants and bulk moduli with respect to the [a]- ([211]-) and [b]- ([220]-) type configurations.

Therefore, the changes within the relaxed lattice total energies clearly reflect the fluctuations in the strain relaxation energy between different atomic configurations. Also this variation seems to become larger when the As concentration increases. The energy associated with the lattice relaxation ($E_{\mathrm{nonrel}} - E_{\mathrm{rel}}$) increases with As concentration.

The linear interpolation between the computed bulk modulus values of GaN and GaAs would give the value of 182 GPa for the 12.5% composition of arsenic. However, table 3 shows that the bulk modulus values from the DFT theory for the [a] and [b] configurations for the same As composition would be some 9% below the linear interpolated value, indicating clearly a nonlinear behaviour of the bulk moduli near the GaN end of the GaAsN alloys.

Although we emphasize that our calculations are for ordered alloys and not for isolated As atoms or As–As pairs, it is still useful to compare and contrast some previous results for those to our calculations. Mattila and Zunger [41] studied As–As impurity pairs in GaN by using a 216-atom supercell and found that the next-nearest-neighbour pairs have the lowest energy out of the six closest pairs. They also found that the As–As pairs in the [200] and [220] cases have low and high energies, respectively. Our results show similar trends in the configurational energies. However, any differences in the ordering of these energies, between our calculations and theirs, can be accounted for as a result of the alloying and use of a small supercell in our calculations.

3.2.1. Band structure. In the following we discuss the modifications occurring in the electronic structure of the GaN crystal with a zinc-blende structure when N sublattice atoms are substitutionally being replaced by isovalent As atoms.

Adding As to the group-V sublattice of GaN between 3.125% and 12.5% reduces drastically the bandgap from its calculated value of 1.93 eV for GaN. We also observe from table 3 that the bandgap values experience large fluctuations within different atomic configurations of As. Although the bandgap fluctuations are large, the lowest-energy configurations of table 3 clearly indicate that the bandgap decreases rapidly for small values of As concentration and then slows down for larger values. Furthermore, all studied As atomic configurations caused a decrease in the bandgap when As concentration was increased, i.e. referring to a redshift in the emission spectra.

It can be seen from the electronic structures in figure 5 that a hybridized impurity band forms in the bandgap for As_1N_{31}, and the same applies for all studied As concentrations and atomic configuration cases. A single isovalent As and As–As impurity pair-related defect states build up into the bandgap of GaN near the VBM in the low-As-concentration limit [21, 41].

We have also studied the pressure dependence of the bandgap in two cases, namely As_1N_{31} and As_2N_{30}[200]. In both cases as the pressure increases the value of the bandgap increases by approximately 0.03 eV GPa^{-1}.

3.2.2. Density of states. From the local densities of states (LDOS) in figure 6 it can be seen that the arsenic impurity states are near the top of the valence band. The localized As derived

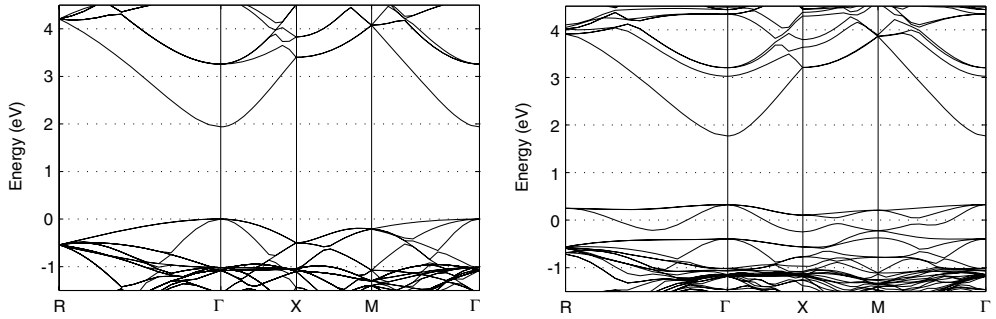

Figure 5. Electronic band structure of GaN (left) and As_1N_{31} (right) along various high-symmetry directions of the Brillouin zone for the simple cubic (sc) $2 \times 2 \times 2$ supercell. The valence band maximum (VBM) of GaN has been chosen as the origin of the (relative) energy scale. For the notation of the configurations see table 1 and figure 1.

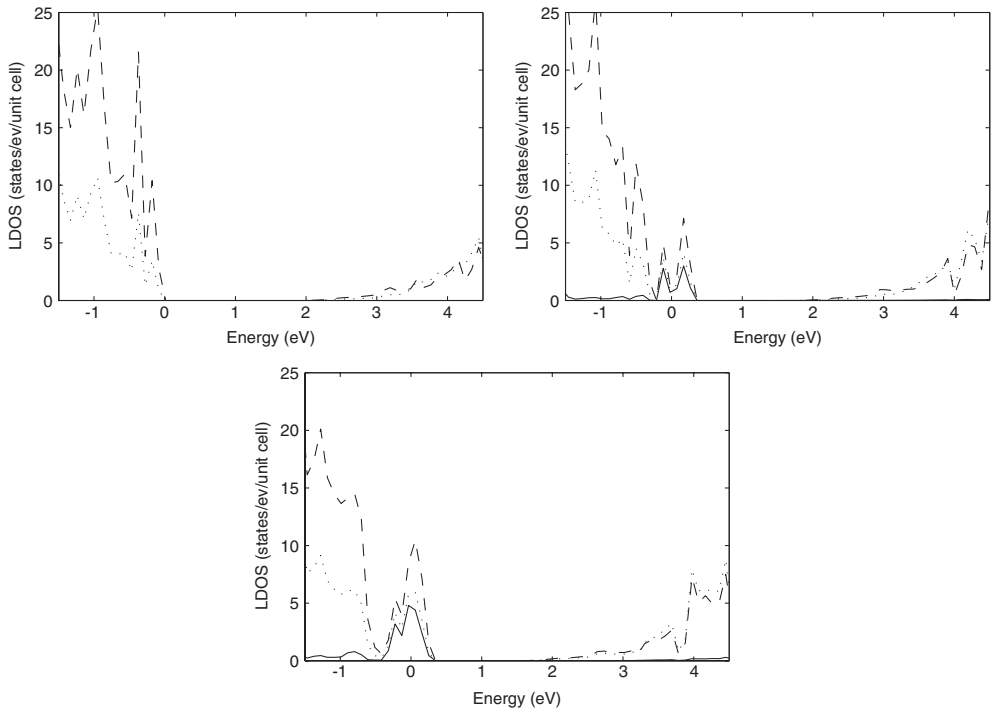

Figure 6. Local densities of states for GaN (top left), As_1N_{31} (top right), and As_2N_{30}[200] (bottom): Ga (dotted line), N (dashed line), and As (solid line). For the notation of the configurations see table 1 and figure 1.

states are hybridized with GaN valence band states, building up the valence band edge for the nondilute arsenic concentrations studied in this work. When arsenic impurities are added to GaN in order to produce a dilute $GaN_{1-y}As_y$ alloy, the formation of the arsenic impurity states reduces the bandgap first very rapidly and then later on more slowly as the arsenic concentration is increased. This could also be seen from the calculated bandgap values and is in agreement with the experimental results [27, 26].

3.3. Arsenic in GaN

In the alloying studies above it has been assumed that arsenic would be on a substitutional N site in N-rich $GaN_{1-y}As_y$ alloy. However, it has been previously predicted theoretically that As would prefer a substitutional Ga site in pure GaN [22].

To investigate the equilibrium energetics for various Fermi level positions we have used the formalism described in [42]. The concentration of a defect in thermodynamic equilibrium is

$$c = N_{\text{sites}} \exp(-E^{\text{f}}/kT), \tag{1}$$

where N_{sites} is the number of possible lattice sites for the defect, k is the Boltzmann constant, and T is the temperature. E^{f} is the formation energy, which can be calculated from

$$E^{\text{f}}[X^q] = E_{\text{tot}}[X^q] - E_{\text{tot}}[\text{GaN, bulk}] - \sum_i n_i \mu_i + q[E_{\text{F}} + E_{\text{v}} + \Delta V]. \tag{2}$$

In this equation $E_{\text{tot}}[X^q]$ is the total energy of the supercell where the impurity has been placed or the defect with charge q (in units of $|e| \equiv 1$) created. $E_{\text{tot}}[\text{GaN, bulk}]$ is the total energy of a corresponding supercell containing bulk GaN. In our study 64-atom and 96-atom supercells have been used in the case of zinc-blende and wurtzite structures, respectively. To take into account the energies of the reservoirs with which the atoms have been exchanged, we need the chemical potentials μ_i of the atoms times their number (n_i is negative if the atom has been removed from the supercell and positive if it has been added). The last term of (2) is the energy of the electron reservoir with which electrons are exchanged. E_{F} is the Fermi energy, which is commonly defined with respect to the top of the valence band [42]. Consequently, the energy of the valence band maximum (E_{v}) of the pure material (GaN) has to be explicitly included in (2). ΔV is a correction term, which aligns the potentials in the defect and bulk supercells. It was not taken into account in the previous theoretical study [22], which can explain some of the differences to the results of the present study. We have calculated the values for the potential correction at an interstitial site in the centre of either Ga or N tetrahedra as far from the impurity atoms as possible in the supercell and as an average over a $3 \times 3 \times 3$ set of points.

We have chosen Ga-rich growth conditions so that the chemical potential of the Ga atoms is calculated from the Ga bulk. The chemical potential of arsenic can be calculated from $\mu_{\text{Ga}} + \mu_{\text{As}} = \mu_{\text{GaAs}}$ assuming equilibrium with GaAs. The chemical potential of nitrogen has been calculated from GaN in a similar fashion.

Our results for As_N and As_{Ga} substitutional defects are presented in table 4. To determine the formation energies using (2) we need the chemical potentials of bulk GaAs, GaN, and Ga, which we have calculated as the total energies per atom pair (GaAs and GaN) or atom (Ga): μ(GaAs, zinc-blende) −9.60 eV, μ(GaN, zinc-blende) −13.93 eV, μ(GaN, wurtzite) −13.94 eV, and μ(Ga) −3.23 eV (calculated in the diamond structure because of the similarity with the zinc-blende structure). We also calculated the cohesive energies of GaN (10.95 eV per Ga–N pair) and GaAs (8.20 eV per Ga–As pair), both in the zinc-blende structure, by referencing the bulk total energies to the energies of the atoms, and we found them to be in good agreement with previous all-electron results (10.88 eV for GaN [43] and 7.99 eV for GaAs [44]). It is also interesting to notice that the differences between the formation energies of the different charge states of the defects behave very similarly in table 4 of our results and table I of [22].

In the wurtzite structure a small structural distortion can be found. The relaxation of the nearest neighbour atoms is different in different directions. Δd_{c} is the relaxation in the direction of the c-axis, while Δd_1 (two atoms) and Δd_2 (one atom) are the changes in the other nearest-

Table 4. The total energy of the supercell E_{tot}, the relaxation of the nearest-neighbour atoms (Δd_c is the relaxation in the direction of the c-axis, while Δd_1 (two atoms) and Δd_2 (one atom) are the relaxations of the other nearest-neighbour atoms), and the formation energy E^f of arsenic on N and Ga sites of the wurtzite and zinc-blende structures of GaN, in different charge states.

	Wurtzite					Zinc-blende		
	E_{tot} (eV)	Δd_1 (%)	Δd_2 (%)	Δd_c (%)	E^f (eV)	E_{tot} (eV)	Δd (%)	E^f (eV)
As_N^0	−662.07	15.4	15.9	16.0	2.90	−438.58	15.2	2.91
As_N^+	−666.01	17.1	17.3	16.5	2.77	−442.61	16.7	2.63
As_N^{2+}	−669.79	18.4	18.4	16.7	2.94	−446.50	17.9	2.59
As_{Ga}^0	−666.86	7.5	9.1	10.2	5.59	−443.28	7.9	5.68
As_{Ga}^+	−672.54	1.2	1.1	1.8	3.74	−449.11	0.9	3.64
As_{Ga}^{2+}	−678.71	−5.1	−5.3	−5.2	1.64	−455.39	−5.2	1.30

neighbour bond lengths in table 4. In both crystal structures the relaxations have large variations depending on the charge of the defect, and this can be seen particularly well in the case of the As_{Ga} defect, where even the direction of the relaxation changes.

We have also calculated thermodynamic transition levels $\epsilon(q_1/q_2)$ for As_N and As_{Ga} defects in various charge states, both for the zinc-blende and wurtzite structures. The transition level $\epsilon(q_1/q_2)$, often called the ionization level, is defined as the Fermi level position where the total energies of two charge states q_1 and q_2 become equal [21, 42]. The transition levels with respect to the valence band maximum (VBM) for As_N defects turn out to be $\epsilon(+/0) = 0.28$ eV and $\epsilon(2+/+) = 0.04$ eV for the zinc-blende structure, while $\epsilon(+/0) = 0.14$ eV and $\epsilon(2+/+) = -0.17$ eV for the wurtzite structure. There seems to be a qualitative difference between the two crystal structures but the value of $\epsilon(2+/+)$ in the zinc-blende structure is very small, which does not allow a definite conclusion to be drawn.

The transition energies for As_{Ga} defects are $\epsilon(+/0) = 2.04$ eV and $\epsilon(2+/+) = 2.33$ eV for the zinc-blende structure, while $\epsilon(+/0) = 1.85$ eV and $\epsilon(2+/+) = 2.10$ eV for the wurtzite structure. It is noticeable that in both crystal structure cases the ordering of the transition states is unusual; i.e., the transition levels with a smaller positive charge are located lower in energy than those with a larger charge. Therefore, the As_{Ga} defect in GaN can be characterized as a negative-U centre, where U refers to the on-site Coulomb repulsion energy [22].

The formation energies of As_{Ga} and As_N in various charge states are presented in figure 7. We find that under Ga-rich conditions arsenic would prefer the substitutional N site over the substitutional Ga site within a large range of Fermi level values (E_F above 0.63 eV). Only in highly p-type material can the concentration of As_{Ga} defects be expected to be equal to or higher than the concentration of As_N defects. The transition energy $\epsilon(+/0)$ for the As_N defect in the wurtzite structure of GaN is only 0.14 eV, and therefore the corresponding As impurity state is close to the VBM. Based on this, we believe that the near-band-edge emission seen in the experiments (where the samples had the wurtzite structure) is related to the As_N defect. The strong band bowing found in our alloy calculations of section 3.2 for the zinc-blende structure can also be expected to be valid in this case. Indeed, this has been confirmed by several recent experiments [27, 26, 29]. The origin of the blue emission is not yet clear, but it seems unlikely that it would be caused by a As_{Ga} defect in Ga-rich conditions (as tentatively proposed in [22]), because of its high formation energy.

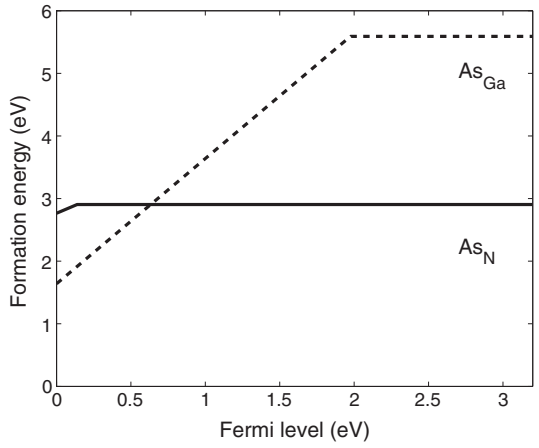

Figure 7. Formation energy of arsenic substitutional defects in GaN in the wurtzite structure under Ga-rich conditions. Only those line segments corresponding to the charge state with the lowest energy at each Fermi level value have been shown in both As_N and As_{Ga} defect cases.

4. Conclusions

We have studied atomic and electronic structures in $GaAs_{1-x}N_x$ and $GaN_{1-y}As_y$ alloys, and transition and formation energies of neutral and charged As substitutional defects in the GaN compound, within the framework of the density functional theory (DFT).

Considering the modifications occurring in the atomic structures of GaAs and GaN, when alloying with N and As, respectively, our calculations show the following. The N atoms, replacing substitutionally As atoms in GaAs, cause the surrounding Ga atoms to relax inwards, making the Ga–N bond length about 15% shorter than the corresponding Ga–As bond length in GaAs. In contrast to this, the As atoms substituting the N atoms in GaN cause the surrounding Ga atoms to move outwards, such that the Ga–As bond length becomes about 15% longer than the corresponding Ga–N bond length in GaN.

Considering the electronic structural properties, we notice first that the relative size of the bandgap fluctuations, for various substitutional impurity atom configurations, is much larger in the $GaAs_{1-x}N_x$ than in the $GaN_{1-y}As_y$ alloys. Therefore, it can be anticipated that the quantum mechanical impurity-to-host state coupling and impurity state localization properties in the case of $GaAs_{1-x}N_x$ alloys are more subtle and difficult to interpret than in the case of $GaN_{1-y}As_y$ alloys.

Our calculations also show that the near-edge conduction band states experience a substantial modification when GaAs is being alloyed with substitutional nitrogen. Notably, fairly large nitrogen localization occurs near the conduction band minimum (CBM). On the other hand, the valence band states near the valence band maximum (VBM) experience hardly any modification due to the alloying. In the case of alloying GaN with substitutional arsenic, the situation becomes quite the opposite. Namely, the conduction band states near the CBM experience only small modifications, while the valence band states near the VBM will undergo changes as arsenic impurity states are induced near the top of the valence band. The As impurity states hybridize with the host GaN states near the VBM in $GaN_{1-y}As_y$, building up the valence band edge of the alloy.

We have also calculated the formation energies and the transition levels of the two possible arsenic substitutional defects in GaN and found that the As atoms prefer the N substitutional site over the Ga site under Ga-rich conditions. The As_N defect has a transition level at 0.14 eV above the valence band maximum in wurtzite GaN and is the most likely cause for the near-band-edge emission found in many experiments.

Acknowledgments

This research has been supported by the Academy of Finland through the TULE-QUEST and Centres of Excellence Programmes. We would like to thank the Centre for Scientific Computing (CSC) in Finland for the computing facilities.

Appendix. Connection between the BEEM technique and the DOS

Ballistic electron emission microscopy (BEEM) is a modification or an extension of scanning tunnelling microscopy (STM). The semiconductor sample to be probed is coated with a thin metal layer. An STM tip is brought near to the surface. Electrons tunnel through the vacuum, move towards the thin metal layer, hopefully not being scattered too much, cross the Schottky barrier, travel through the semiconductor film to be studied, and are finally collected at the other end of the sample. The thin metal layer is needed to control the electron energy entering the semiconductor, by changing the bias voltage.

The BEEM method is capable of probing separately the conduction- and valence-band structures. Therefore, it works as a complementary tool to optical studies, where interband transitions are involved.

The BEEM current I_c flowing through the sample can approximately be expressed as

$$I_c \sim \int_{E_F}^{E_F+eV_T} \rho_m(E)\rho_{sc}(E)\,dE, \tag{A.1}$$

where V_T is the tip bias voltage, and $\rho_m(E)$ and $\rho_{sc}(E)$ are the electronic densities of states for the metal and the semiconductor, respectively. Differentiating this once with respect to the bias voltage yields

$$\frac{dI_c}{dV_T} \sim \rho_m(E_F + eV_T)\rho_{sc}(E_F + eV_T). \tag{A.2}$$

The usual BEEM $I_c(V_T)$ curve is monotonically increasing, with different regions clearly distinguishable (see e.g. figure 1 of [30]). Differentiating the BEEM current I_c once with respect to V_T (see (A.2)) gives something that corresponds to the actual DOS of the material [45]. Therefore, the BEEM current corresponds to the integrated DOS. If dI_c/dV_T is differentiated once more with respect to V_T we obtain the second-derivative BEEM (SD-BEEM) spectra [30].

Considering the GaAs conduction band, the Γ valley is the lowest one, followed by the L and X valleys, about 0.3 and 0.5 eV above the conduction band minimum at the Γ point, respectively. The fingerprint of these valleys in the $I_c(V_T)$ curve is represented by the sudden increases in its slope, i.e. in the first-derivative BEEM spectra, when a new valley is contributing to the BEEM spectra as the voltage V_T becomes larger (see figure 1 of [30]). Consequently, these abrupt increases in the first-derivative BEEM spectra (or in the DOS function) manifest themselves as peaks in the second-derivative BEEM spectra (see figure 2 of [30]). The SD-BEEM measurements for GaAs by Kozhevnikov *et al* [30] show two peaks, namely the Γ- and L-like peaks, which are about 0.3 eV apart from each other. Our electronic band structure calculations for GaAs (not shown) reproduce well the same value for the distance between these peaks.

References

[1] Vurgaftman I and Meyer J R 2003 *J. Appl. Phys.* **94** 3675
[2] Bellaiche L, Wei S-H and Zunger A 1997 *Appl. Phys. Lett.* **70** 3558

[3] Foxon C T, Cheng T S, Novikov S V, Lacklison D E, Jenkins L C, Johnston D, Orton J W, Hooper S E, Baba-Ali N, Tansley T L and Tret'yakov V V 1995 *J. Cryst. Growth* **150** 892
[4] Bi W G and Tu C W 1997 *Appl. Phys. Lett.* **70** 1608
[5] Neugebauer J and Van de Walle C G 1995 *Phys. Rev.* B **51** 10568
[6] Wei S-H and Zunger A 1996 *Phys. Rev. Lett.* **76** 664
[7] Carrier P, Wei S-H, Zhang S B and Kurtz S 2005 *Phys. Rev.* B **71** 165212
[8] Salzman J and Temkin H 1997 *Mater. Sci. Eng.* B **50** 148
[9] Bandić Z Z, Hauenstein R J, O'Steen M L and McGill T C 1996 *Appl. Phys. Lett.* **68** 1510
[10] Goldman R S, Feenstra R M, Briner B G, O'Steen M L and Hauenstein R J 1996 *Appl. Phys. Lett.* **69** 3698
[11] Perkins J D, Mascarenhas A, Zhang Y, Geisz J F, Friedman D J, Olson J M and Kurtz S R 1999 *Phys. Rev. Lett.* **82** 3312
[12] Bellaiche L, Wei S-H and Zunger A 1996 *Phys. Rev.* B **54** 17568
[13] Lowther J E, Estreicher S K and Temkin H 2001 *Appl. Phys. Lett.* **79** 200
[14] Orellana W and Ferraz A C 2001 *Appl. Phys. Lett.* **78** 1231
[15] Li W, Pessa M and Likonen J 2001 *Appl. Phys. Lett.* **78** 2864
[16] Ahlgren T, Vainonen-Ahlgren E, Likonen J, Li W and Pessa M 2002 *Appl. Phys. Lett.* **80** 2314
[17] Fan W J, Yoon S F, Ng T K, Wang S Z, Loke W K, Liu R and Wee A 2002 *Appl. Phys. Lett.* **80** 4136
[18] Zhang S B and Wei S-H 2001 *Phys. Rev. Lett.* **86** 1789
[19] Kent P R C and Zunger A 2001 *Phys. Rev.* B **64** 115208
[20] Arola E, Ojanen J, Komsa H-P and Rantala T T 2005 *Phys. Rev.* B **72** 045222
[21] Mattila T and Zunger A 1998 *Phys. Rev.* B **58** 1367
[22] Van de Walle C G and Neugebauer J 2000 *Appl. Phys. Lett.* **76** 1009
[23] Ramos L E, Furthmüller J, Leite J R, Scolfaro L M R and Bechstedt F 2003 *Phys. Rev.* B **68** 085209
[24] Novikov S V, Winser A J, Bell A, Harrison I, Li T, Campion R P, Staddon C R, Davis C S, Ponce F A and Foxon C T 2002 *J. Cryst. Growth* **240** 423
[25] Foxon C T, Novikov S V, Li T, Campion R P, Winser A J, Harrison I, Kappers M J and Humphreys C J 2003 *J. Cryst. Growth* **251** 510
[26] Kimura A, Paulson C A, Tang H F and Kuech T F 2004 *Appl. Phys. Lett.* **84** 1489
[27] Kimura A, Tang H F and Kuech T F 2004 *J. Cryst. Growth* **265** 71
[28] Wu J, Walukiewicz W, Yu K M, Denlinger J D, Shan W, Ager J W III, Kimura A, Tang H F and Kuech T F 2004 *Phys. Rev.* B **70** 115214
[29] Tsuda Y, Mouri H, Yuasa T and Taneya M 2004 *Appl. Phys. Lett.* **85** 4361
[30] Kozhevnikov M, Narayanamurti V, Reddy C V, Xin H P, Tu C W, Mascarenhas A and Zhang Y 2000 *Phys. Rev.* B **61** R7861
[31] Kresse G and Joubert D 1999 *Phys. Rev.* B **59** 1758
[32] Perdew J P and Zunger A 1981 *Phys. Rev.* B **23** 5048
[33] Perdew J P, Chevary J A, Vosko S H, Jackson K A, Pederson M R, Singh D J and Fiolhais C 1992 *Phys. Rev.* B **46** 6671
[34] Yu P Y and Cardona M 2001 *Fundamentals of Semiconductors* (Berlin: Springer)
[35] McKay H A, Feenstra R M, Schmidtling T and Pohl U W 2001 *Appl. Phys. Lett.* **78** 82
[36] Ciatto G, d'Acapito F, Sanna S, Fiorentini V, Polimeni A, Capizzi M, Mobilio S and Boscherini F 2005 *Phys. Rev.* B **71** 115210
[37] Uesugi K, Suemune I, Hasegawa T, Akutagawa T and Nakamura T 2000 *Appl. Phys. Lett.* **76** 1285
[38] Bentoumi G, Timoshevskii V, Madini N, Côté M, Leonelli R, Beaudry J-N, Desjardins P and Masut R A 2004 *Phys. Rev.* B **70** 035315
[39] Al-Yacoub A and Bellaiche L 2000 *Phys. Rev.* B **62** 10847
[40] Bell L D and Kaiser W J 1988 *Phys. Rev. Lett.* **61** 2368
[41] Mattila T and Zunger A 1999 *Phys. Rev.* B **59** 9943
[42] Van de Walle C G and Neugebauer J 2004 *J. Appl. Phys.* **95** 3851
[43] Fiorentini V, Methfessel M and Scheffler M 1993 *Phys. Rev.* B **47** 13353
[44] Filippi C, Singh D J and Umrigar C J 1994 *Phys. Rev.* B **50** 14947
[45] Ludeke R 1993 *Phys. Rev. Lett.* **70** 214